SAND2015-2757C

Effects of Atwood number on Kelvin-Helmholtz Instabilities Formed from Oblique Shock Interaction with a Heavy Gas Column

Jason H. Yoo[1]
The University of New Mexico, Albuquerque, New Mexico, 87131

Abstract

Oblique shockwave interactions with a cylindrical heavy gas column produce counter-rotating vortex pairs, indicative of the Richtmyer-Meshkov instability (RMI), as well as periodic co-rotating vortices congruent with Kelvin-Helmholtz instabilities (KHI). Previous experiments conducted at the Shock Tube Facility at the University of New Mexico (UNM) have shown that the respective wavelength of the KHI varies with Mach number, but also with the inclination of the heavy gas column with respect to the shock front. An oblique shockwave is simulated by tilting the shock tube at a 20 degree angle with respect to horizontal, while the initial conditions (ICs) are introduced vertically into the test section and driven by gravity. Visualization of the shock-accelerated column of heavy gas is achieved by using Planar Laser-Induced Fluorescence (PLIF) imaging. Vertical (wall normal) PLIF images reveal KHI that begin as small perturbations along the upstream side, but quickly grow into full "cat's eye" vortices that cascade down the entire vertical length of the gas column. For data collected with a Mach = 1.67 shockwave and 20 degree angle of inclination, it was found that the wavelength of the KHI and the time over which these vortices develop are Atwood number dependent. Atwood number describes the relative difference in densities between the cylindrical heavy gas column and surrounding air.

Nomenclature

A	=	Atwood Number
a	=	speed of sound in air
AOI	=	area of interest
CCD	=	charge-coupled device
CRVP	=	counter-rotating vortex pair
Δt	=	time between pressure pulses
ICs	=	Initial Conditions
KHI	=	Kelvin-Helmholtz instability
l	=	distance between two pressure transducers
λ	=	wavelength
m	=	mass
Nd:YAG	=	Neodymium-doped Yttrium Aluminum Garnet
PLIF	=	Planar Laser Induced Fluorescence
P	=	pressure
ρ	=	density
R	=	gas constant
RMI	=	Richtmyer-Meshkov instability

[1] Undergraduate Research Assistant, Mechanical Engineering Dept., 1 University of New Mexico, Albuquerque, NM, 87131, AIAA Student Member

SF_6 = sulfur-hexafluoride
T = temperature
V_s = velocity of shock front
V = volume of the tank

I. Introduction

RICHTMYER-Meshkov instabilities (RMI) are hydrodynamic instabilities that develop when an interface between two fluids of different densities is impulsively accelerated. This impulsive acceleration can be due to an impulsive body force, or by a passing shock wave. This instability was first theoretically described by Richmyer[1] and later demonstrated experimentally by Meshkov.[2] Understanding of RMI can be an important asset in many engineering challenges. RMI occurs in various natural and engineering phenomena, such as evolution of supernova remnants,[3] fuel mixing in scramjet engines,[4] and inertial confinement fusion.[5] Another well-known hydrodynamic instability besides RMI is the Kelvin-Helmholtz Instability (KHI). KHI was first introduced by Hermann von Helmholtz in 1868,[6] and later by Lord Kelvin in 1871.[7] KHI develop when there is a significant velocity difference across the interface between two fluids. Shear due to the velocity difference results in the formation of "cat's eye" vortices on the interface. Kelvin-Helmholtz instabilities result from plasma ignition in inertial confinement fusion,[8] have been observed in the cloud bands of Saturn and Jupiter, and are present in the sun's corona.[9]

The most recent experiments conducted at the shock tube facility at the University of New Mexico have been focused on oblique shock interactions with a column of heavy gas, specifically sulfur-hexafluoride (SF_6). The shock-accelerated gas columns reveal the expected evolution of Richtmyer-Meshkov instabilities, but also unexpected small-scale features, similar in morphology to Kelvin-Helmholtz instabilities that develop on the trailing edge of the column. These instabilities present themselves as periodic waves that seem to grow with time and evolve into vortices that cascade down the entire length of the gas column. The respective wavelength of the KHI varies with Mach number, with the inclination of the heavy gas column with respect to the shock front,[10] but also seems to depend on the Atwood number of the experiment. Acetone was used in experiments because it is excited to fluorescence by laser illumination, specifically under ultraviolet light between 225 nm and 320 nm.[11] Planar Laser Induced Fluorescence (PLIF) images were collected at downstream locations by triggering camera exposure with delay generators. This paper focuses on these small-scale Kelvin-Helmholtz instabilities, a description of how the data was analyzed, and a detailed description of the periodic behavior, including Atwood number dependence.

II. Experimental Setup

Experimental data presented in this paper were collected from University of New Mexico (UNM) shock tube facility. The shock tube group at UNM is dedicated primarily to the study of Richtmyer-Meshkov Instabilities (RMI), specifically as a result of shock interaction with a column of SF_6 infused with acetone. A horizontal representation of the tube is given in Fig.1. The shock tube itself is comprised of four main sections: the driver section, the driven section, the test section and run-off section. All but the driver section are filled with air at room temperature and pressure. The driver section is separated from the driven section by a thin polyester diaphragm film and pressurized with helium to a predetermined pressure, depending on the desired Mach number. When triggered, a pneumatically-driven stainless steel rod tipped with a broad arrowhead punctures the diaphragm, sending a planar normal shock in air down the length of the tube. Two high-frequency response pressure transducers, located 2.60 meters apart on the top of the driven section, record the pressure pulse of the shock wave as it passes. NI-Scope software and a digital oscilloscope are used to record the pressure data, providing the necessary information to determine the velocity of the shock via Eqn.1, where Δt is the time between pressure pulses and l is the distance between the pressure transducers (2.60 m). The Mach number can then be calculated using Eqn. 2, where a is the local speed of sound in air.

$$V_s = \frac{\Delta t}{l} \tag{1}$$

$$M = \frac{V_s}{a} \tag{2}$$

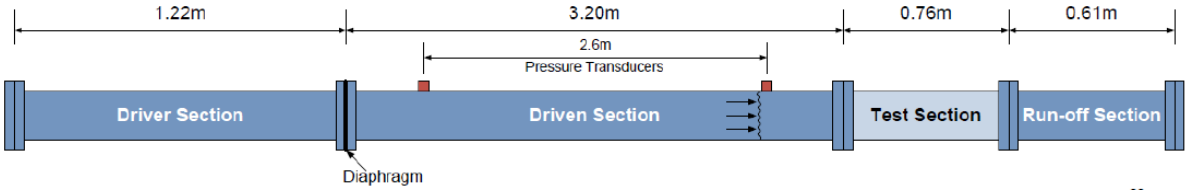

Figure 1. Representation of the horizontal Shock Tube Setup. Flow direction is from left to right.

A. Initial conditions and Atwood Number

The governing parameter of this experiment is the Atwood number. The Atwood number is a dimensionless density ratio defined as

$$A = \frac{\rho_1 - \rho_2}{\rho_1 + \rho_2} \tag{3}$$

where ρ_1 and ρ_2 are the densities of the heavy and light gases, respectively. Previous studies have shown that the growth rate of RMI is found to be greater in experiments with higher Atwood numbers (as A approaches unity, the growth rate of RMI increases).[12] Atwood number variation has also been found to have an effect on the morphology of the instabilities as they grow with time.[13] Initial conditions (ICs) consist of one of two types, depending on the desired Atwood number. The first type is a pure SF_6/acetone mixture, which corresponds to a maximum Atwood number of 0.67. The second type of initial conditions consists of a mixture of SF_6 and nitrogen, infused with acetone. The concentration of nitrogen in the SF_6/nitrogen mixture determines the effective Atwood number. As the Atwood number decreases, the mass fraction of nitrogen in the mixture increases. Table 1 is the known constant values used in calculations regarding the mass fraction of nitrogen and SF_6 according to Atwood number.

Table 1. Known constant values used in Atwood number *A*= 0.50 calculation.

	Gas Constants, R (J/kg·k)	Compressibility Factor, Z	Partial Pressure, P (KPa)
N_2	297	1	2116.69
SF_6	56.927	0.98	380.78
Air	287	N/A	87.3
Volume, V (m^3)	0.0433	**Temperature, T (K)**	300

$$\boldsymbol{m_{SF_6} = \frac{P_{SF_6} \cdot V}{Z_{SF_6} \cdot R_{SF_6} \cdot T} = 0.984kg, \quad m_{N_2} = \frac{P_{N_2} \cdot V}{Z_{N_2} \cdot R_{N_2} \cdot T} = 1.028kg \quad \rightarrow \quad m_{total} = m_{SF_6} + m_{N_2} = 2.012kg}$$

$$\boldsymbol{m_{ratio_{SF_6}} = \frac{m_{SF_6}}{m_{total}} = 0.489, \qquad m_{ratio_{N_2}} = \frac{m_{N_2}}{m_{total}} = 0.511 \quad \rightarrow \quad m_{ratio_{SF_6}} + m_{ratio_{N_2}} = 1}$$

$$\boldsymbol{\rho_{SF_{6atm}} = \frac{P_{atm}}{Z_{SF_6} \cdot R_{SF_6} \cdot T} = 5.001 \frac{kg}{m^3} \qquad \rho_{N_{2atm}} = \frac{P_{atm}}{Z_{N_2} \cdot R_{N_2} \cdot T} = 0.946 \frac{kg}{m^3}}$$

$$\boldsymbol{\rho_{IC} = m_{ratio_{SF_6}} \cdot \rho_{SF_{6atm}} + m_{ratio_{N_2}} \cdot \rho_{N_{2atm}} = 2.93 \frac{kg}{m^3}}$$

$$\boldsymbol{A = \frac{\rho_{IC} - \rho_{air}}{\rho_{IC} + \rho_{air}} = \frac{2.93 \frac{kg}{m^3} - 0.979 \frac{kg}{m^3}}{2.93 \frac{kg}{m^3} + 0.979 \frac{kg}{m^3}} = 0.499}$$

where *V* is the volume of the tank. Any Atwood number between 0 and 1 can be found by varying the corresponding partial pressures for nitrogen and SF_6.

The mixture of heavy gas is injected vertically downward into the test section and is stabilized using a co-flow of air. The mixture flows through a flow straightener before being injected into the test section. This flow straightener is used to maintain a uniform, laminar jet, traveling approximately at 1.2 m/s. This speed is maintained via a regulator attached to the tank housing the ICs. The injection tube itself is made out of 6 mm inner diameter (i.d.) stainless steel, centered inside a 15mm i.d. acrylic co-flow tube.

In order to visualize ICs, and subsequent shock-accelerated gas column, acetone gas, which fluoresces under UV light, is used as a tracer. This is accomplished by allowing the sulfur-hexafluoride (SF_6) to bubble through a Pyrex flask of pure liquid acetone prior to injection into the test section. The acetone itself takes up a small fraction of the heavy gas; approximately 11%.[12] It is important to note that the density of the heavy gas, and corresponding Atwood number calculations do not take this into account. The reason for this is because density calculations of a three-species mixture can be incredibly complex. For the purposes of this paper, the mass fraction of acetone in the ICs is neglected.

B. Oblique Shock Generation and Optics

The shock tube was initially oriented in the horizontal position (0 degree) for the study of normal shock wave interactions. In order to analyze the instabilities caused by an oblique shock wave, the shock tube had to be tilted to a 20 degree angle with respect to horizontal. Because of this inclination, the normal shock propagating down the shock tube effectively simulates an oblique shock as it impacts the heavy gas column. Figure 2 a) is an image of the test section with injection tube and an illustration of shock front relative to the ICs.

Two sets of Neodimium-Doped Ytrium Aluminum Garnet (Nd:YAG) lasers are used to visualize the shock-accelerated column. The 266 nm wavelength (ultra-violet part of the light spectrum) laser beam is formed into a 1 mm wide sheet by passing the beam through a combination of cylindrical and spherical glass lenses. Duration of the laser pulse depends on the laser being used; either 5 ns or 10 ns. The lasers are triggered by the downstream pressure transducer on top of the driven section of the shock tube. Figure 2 b) is an image of the laser and optical set up. PLIF images are taken using a four megapixel Apogee Alta U42 cooled CCD (charge-coupled device) astronomy camera. Time resolved images are obtained via the timings set on the delay generator, which coincide with the exposure on the camera.

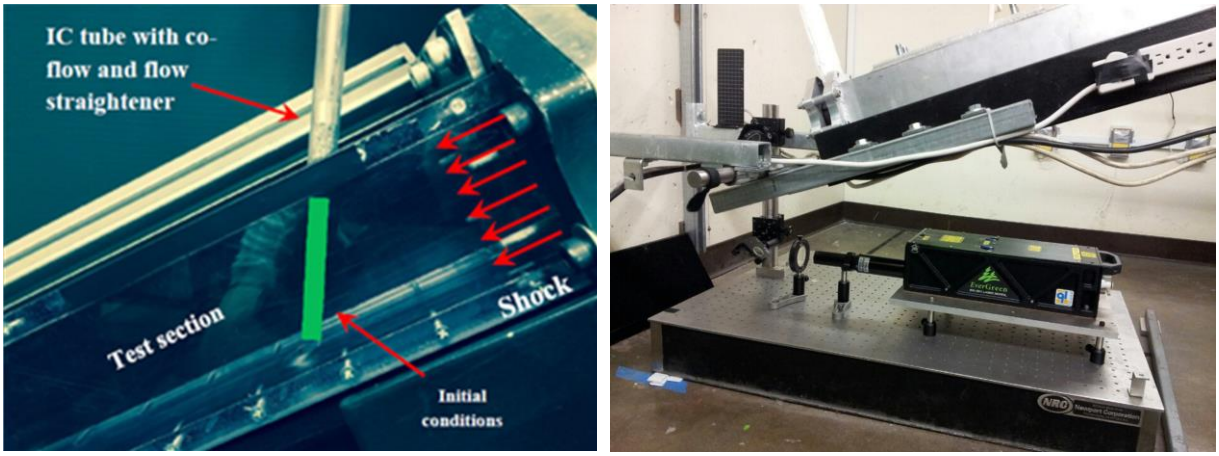

a) **b)**

Figure 2. Illustration of the Oblique Shock with respect to the ICs. Shock direction is from right to left (a). Optical and Laser Setup (b).

III. Results and Discussion

Vorticity deposition on the shock-accelerated gas column occur through two main mechanisms. The first is baroclinic vorticity. As the shock wave impacts and compresses the heavy gas column, the misalignment of pressure and density gradients deposits three-dimensional vorticity on the interface, which is shown in Fig. 3 a. The second

mechanism is shear between the gas column and the air behind it, which is moving at piston velocity. Most of the air passes around the column, but a component of that air impacts the upstream side of the column and travels down its entire vertical length (see Fig. 3 b). The difference in velocity between the air and the column of SF_6 causes shear, which fuels the instabilities, inducing vortex roll-up indicative of KHI.[10]

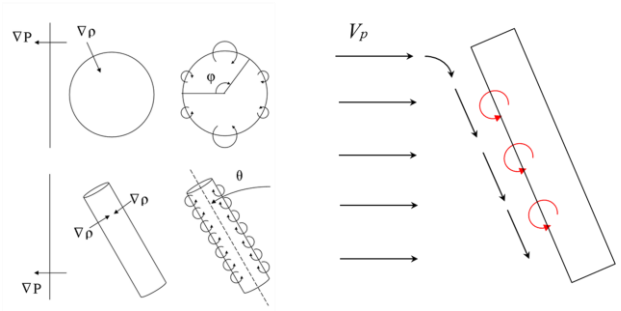

a) **b)**

Figure 3. Schematics showing a) deposition of baroclinic vorticity, and b) vorticity produced by shear.[10]

A number of experiments were conducted in the shock tube facility at UNM over approximately 18 months. Several of these experiments focused on how changes in Atwood number affected the morphology of the shock-accelerated gas column, in both vertical and centerline plane. A schematic of these planes is shown in Fig. 4. Three separate Atwood numbers were chosen; 0.25, 0.50, and 0.67. An Atwood number of 0.67 corresponds to pure SF_6 initial conditions.

While KHI do present in the centerline plane as a secondary instability to traditional RMI, this paper focuses on KHI that develop along the upstream edge of the gas column in the vertical plane. Figure 5 is an image showing the development of KHI in this plane. Analysis and measurements of the instabilities were taken within the area of interest (AOI) shown. The entire vertical height of the image is 5 cm. The AOI is approximately 1.60 cm in width and 2.20 cm in height. Although it is clear that KHI develop along the entire vertical length of the column, all measurements of the wavelengths of the instabilities were taken within this AOI. This area was specifically chosen for analysis because the level of detail is generally better in the centers of each image and because effects of the wall have minimal impact on the instabilities in this region. The false colors used in the images are a method of increasing detail and emphasizing small-scale features that would normally be missed. The light colored region (white/yellow) represents high concentration of initial conditions, while the black region corresponds to pure air.

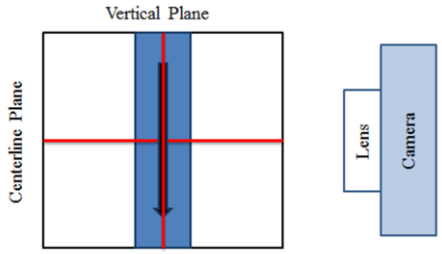

Figure 4. Schematic of vertical and centerline planes in test section cross-section with respect to camera position.

A. Qualitative Analysis

A sequence of images for an inclination angle of 20 degrees, Atwood number of 0.50, and Mach number 1.67 is shown in Fig. 6. These chronologically ordered images reveal temporal evolution of the gas column after shock impact. The camera used to take these images is oriented parallel with the test section. Therefore, the column seems tilted 20 degrees and the shock appears vertical. In reality, the ICs are injected vertically into the test section, driven by gravity.

The timings shown in each image are with respect to shock impact. At t = 0 μs, the shock is in the center of the ICs. The shock first reaches the column at the top of the images, and then quickly propagates downstream. The shock has passed out of view in all images collected downstream at times later than t = 0 μs. The high density region behind (upstream) the shock shows compression of the gas column as the shock wave propagates downstream. At time t = 87 μs, the shock has passed through the column completely. At t = 117 μs the large counter-rotating vortex pair (CRVP) inherent in RMI begin to develop downstream of the high density region. The Kelvin-Helmholtz waves begin to appear at

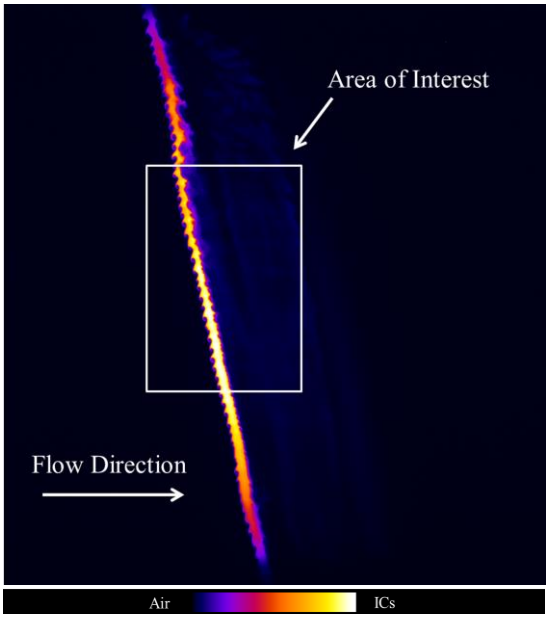

Figure 5. Representative image showing area of interest.

approximately t = 163 μs after shock impact. First presenting as small perturbations along the upstream interface, the waves continue to grow and evolve into full "cat's eye" vortices (t = 335 μs) that cascade down the column. The waves then begin to combine and effectively double in wavelength (530 μs) before mixing and transitioning to turbulence at ~ 627 μs after shock impact.

Similar trends were observed in images collected for Atwood numbers A = 0.25 and 0.67, with one notable difference. The small perturbations along the interface developed at different times for each Atwood number. This in turn, affected the development of the KH waves. As the Atwood number increases, the longer it takes for the waves to begin to develop on the trailing edge. Figure 7 is an image showing when the waves first begin to develop for each Atwood number. For Atwood = 0.25, the waves first present at t = 288 μs, however for Atwood numbers 0.50 and 0.67, the waves began to appear at t = 163 μs and t = 58 μs, respectively. Also, the linear distance between the centers of the vortices seems to increase with decreasing Atwood number. A comparison of fully developed vortices at different Atwood numbers (as labeled) is shown in Fig. 8. The selection of images in Fig. 8 were specifically chosen based on fully developed Kelvin-Helmholtz waves, prior to merging and transition to turbulence. Notice that even to the naked eye, the distance between a pair of vortices and their individual size seems to decrease as the Atwood number of the experiment increases. These properties of the flow suggest that the growth rate of the KHI depends on the Atwood number of the experiment.

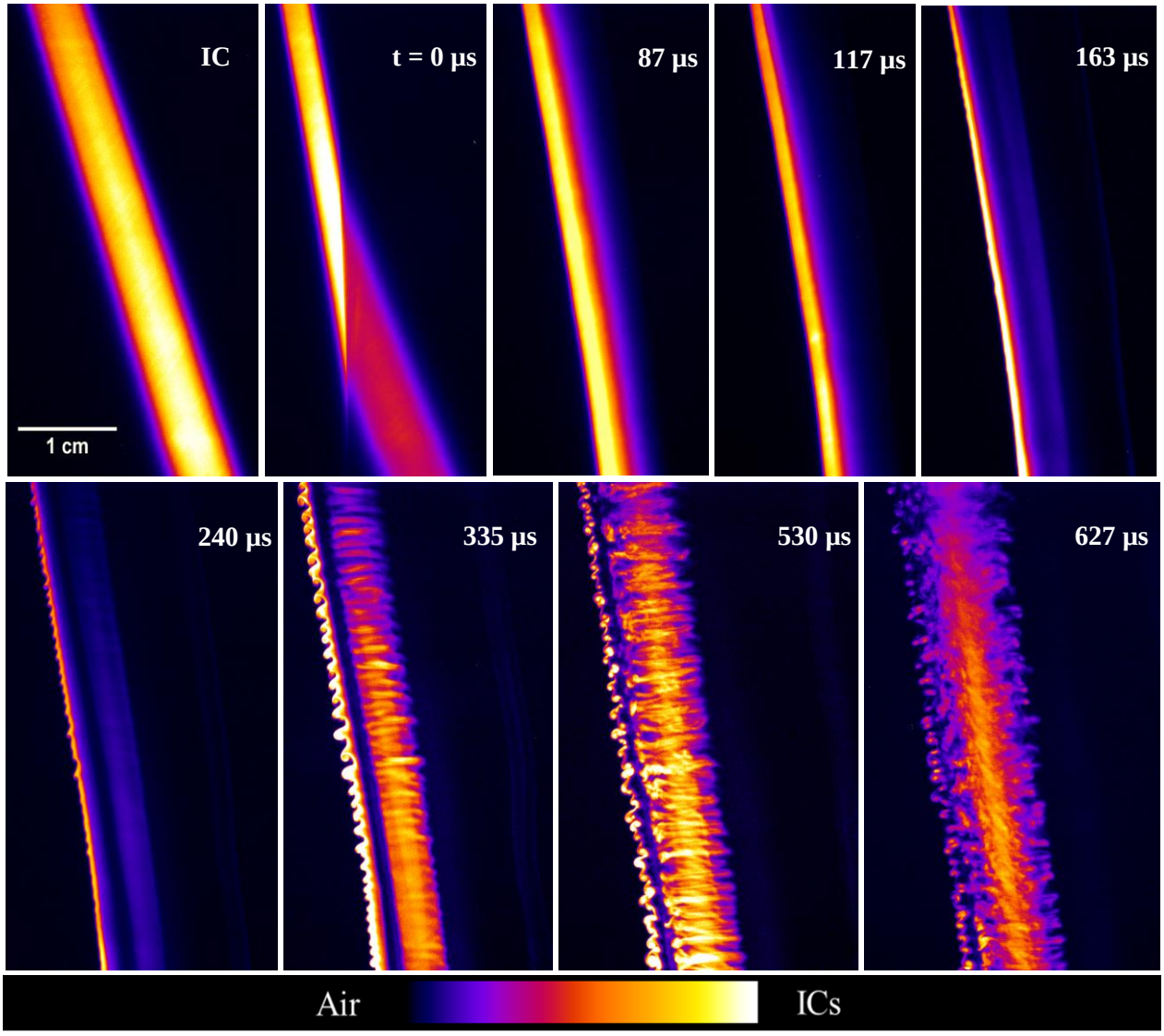

Figure 6. Temporal evolution of the heavy gas column at M = 1.67 shock wave and 20° inclination for Atwood number A = 0.50, (flow direction from left to right).

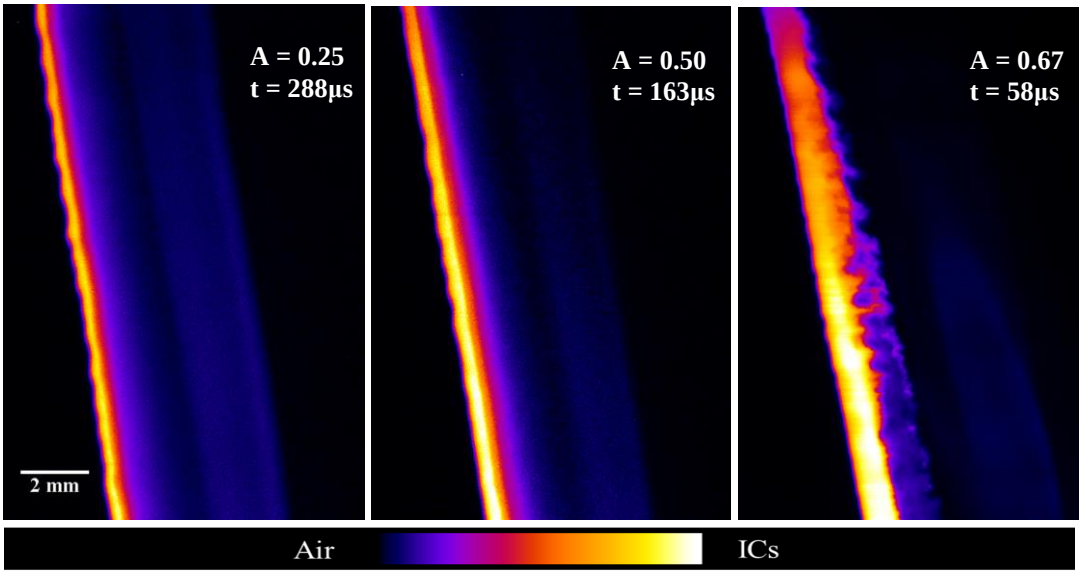

Figure 7. Beginning of Kelvin-Helmholtz wave formation at Mach = 1.67 shockwave with different Atwood numbers (flow from left to right).

B. Quantitative Analysis

The quantitative parameter of interest in this section is the wavelength, λ, of the KHI. Although there are not yet enough samples to create statistical data, this analysis will aid in the understanding of the formation and evolution of these instabilities on the trailing edge of the column. Wavelengths are measured as the linear distance between the centers of a pair of fully developed vortices. Although there appear to be a large number of possible measurements within the AOI, not all of the images analyzed have the same number of these measurements. Therefore, a total of 5 measurements of consecutive vortices were taken with the AOI of each image and averaged. These data include three Atwood numbers (0.25, 0.50, and 0.67) and a Mach number of 1.67.

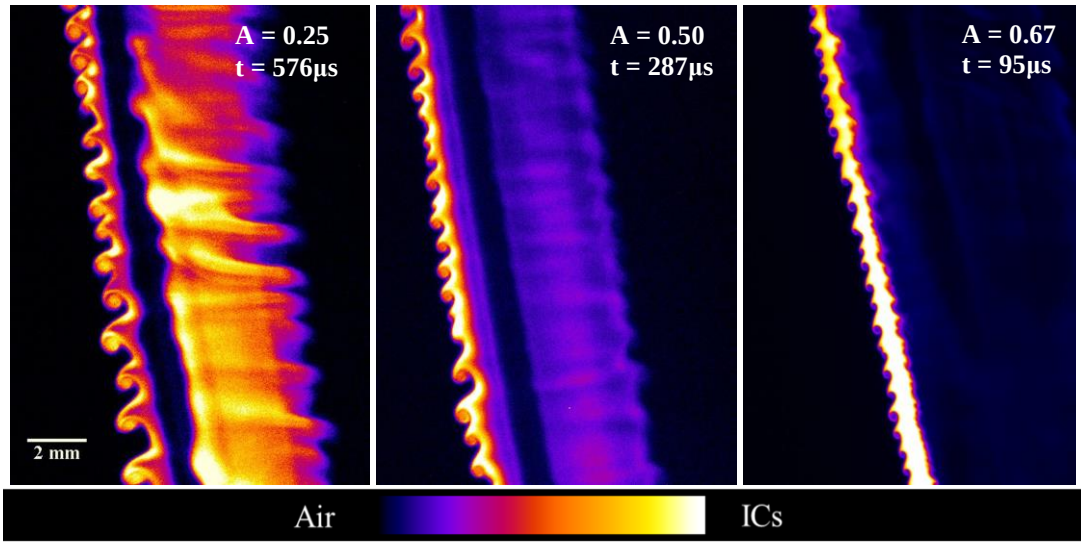

Figure 8. Comparison of KHI vortices at different Atwood number for 20° inclined shock tube (flow from left to right).

Dimensionless wavelengths versus Atwood number are plotted in Fig. 9. Each wavelength is normalized by the diameter of the initial conditions, D_{IC} = 6.35 mm. Error bars of ±5% indicate uncertainty in the computed Atwood number due to effects of acetone in ICs. Without further investigation into the exact Atwood number of each experiment, it is impossible to determine the error in Atwood number. Therefore a level of confidence of 95% is assumed.

Standard deviations about the mean of the averaged wavelengths were calculated from the data and added as vertical error bars to the graph. The curve fit seen as a red line was added not as a definitive prediction of the wavelengths between the known values of Atwood number, but as a visual aid to show a downward trend. It is clear that the wavelengths of the KHI do depend on Atwood number, especially as the Atwood number is increased from 0.50. These results will be supplemented with more data as experiments progress.

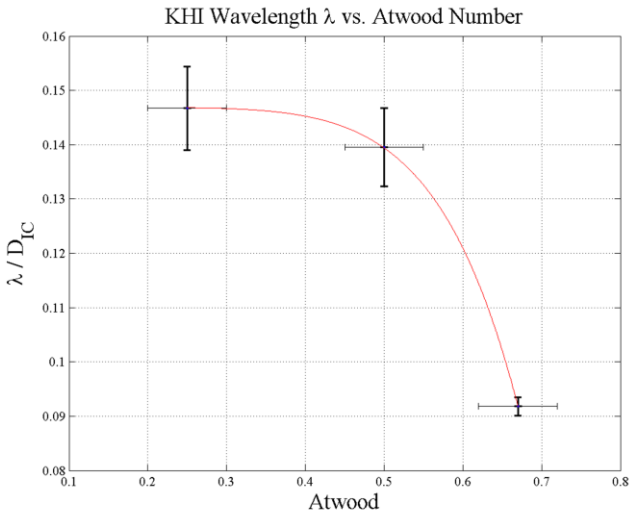

Figure 9. Normalized KH wavelength as a function of Atwood number.

IV. Conclusion

This paper presents experimental results of the effects of Atwood number on Kelvin-Helmholtz Instabilities formed from oblique shock interaction with a heavy gas column. Experiments were performed at the University of New Mexico tiltable shock tube facility. It has been found that the growth rate of the instabilities increases as Atwood number is increased. This corresponds to larger wavelengths for lower Atwood numbers. Future experiments will provide more statistical data for KHI with respect to Atwood number at a 20° angle of inclination as well as other inclination angles; 15 degrees and 10 degrees.

Acknowledgments

This research is supported by NNSA grant DE-NA0002220. The author thanks Dr. C. Randall Truman and Dr. Peter Vorobieff for their support, as well as Patrick Wayne and Captain Dell Olmstead for their mentorship during this study. Additional thanks go to the other members of the UNM shock tube team: D. Simons, L. Smith, E. Keller, D. Davis for their time spent collecting data and improving the testing rig, and to the UNM ME department machine shop for all their support.

References

[1]Richtmyer, Robert D. "Taylor instability in shock acceleration of compressible fluids." *Communications on Pure and Applied Mathematics* 13.2 (1960): 297-319.

[2]Meshkov, E. E. "Instability of the interface of two gases accelerated by a shock wave." *Fluid Dynamics* 4.5 (1969): 101-104.

[3]Arnett, David. "The role of mixing in astrophysics." *The Astrophysical Journal Supplement Series* 127.2 (2000): 213.

[4]Yang, Q., Chang, J., Bao, W., "Richtmyer-Meshkov Instability Induced Mixing Enhancement in the Scramjet Combustor with a Central Strut." *Advances in Mechanical Engineering* 6 (2014): 614189.

[5]Yang, Joseph, Toshi Kubota, and Edward E. Zukoski. "Applications of shock-induced mixing to supersonic combustion." *AIAA Journal* 31.5 (1993): 854-862.

[6]Helmholtz, H., "On the discontinuous movements of fluids." *Monthly Reports of the Royal Prussian Academy of Philosophy in Berlin* 23 (1868): 215–228.

[7]Thomson (Lord Kelvin), W., "Hydrokinetic solutions and observations." *Philosophical Magazine* 42 (1871): 362–377

[8]Hurricane, O., Hansen, J., Robey, H., Remington, B., Bono, M., Harding, E., Drake, R., Kuranz, C., "A high energy density shock driven Kelvin-Helmholtz shear layer experiment." *Physics of Plasma* 16 (2009): 056305.

[9]Broad, W., "In Deep Sea, Waves With A Familiar Curl." *The New York Times*, 19 April 2010, URL: http://www.nytimes.com/2010/04/20/science/20waves.html.

[10]Wayne, P., Olmstead, D., Vorobieff, P., Truman, C.R., Kumar, S. "Oblique shock interaction with a cylindrical density interface." *8th International Conference on Computational and Experimental Methods in Multiphase and Complex Flow*, Multiphase Flow 2015, Valencia, Spain, April. 2015.

[11]Tran, T., Kochar, Y., Seitzman, J., " Measurements of Liquid Acetone Fluorescence and Phosphorescence for Two-Phase Fuel Imaging." *43rd Aerospace Sciences Meeting and Exhibit*, Reno, NV, Jan. 2005, AIAA 2005-0827

[12]Olmstead, D., Wayne, P., Kumar, S., Truman, C.R., Vorobieff, P., "Experimental Study of Shock Accelerated Inclined Heavy Gas Cylinder." Submitted to *Journal of Fluid Mechanics* (2015).

[13]Anderson, M., "Oblique Shock Interactions With Perturbed Density Interfaces," Ph.D. Dissertation, Mechanical Engineering Dept., The University of New Mexico (2011).